Tough and dense boron carbide obtained by high-pressure (300 MPa) and low-temperature (1600°C) spark plasma sintering

Badica, Petre; Grasso, Salvatore; Borodianska, Hanna; Xie, Sky Shumao; Li, Peifeng; Tatarko, Peter; Reece, Mike J.; Sakka, Yoshio; Vasylkiv, Oleg

2014

Badica, P., Grasso, S., Borodianska, H., Xie, S. S., Li, P., Tatarko, P., et al. (2014). Tough and dense boron carbide obtained by high-pressure (300 MPa) and low-temperature (1600^|^deg;C) spark plasma sintering. Journal of the Ceramic Society of Japan, 122(1424), 271-275.

https://hdl.handle.net/10356/105276

https://doi.org/10.2109/jcersj2.122.271

Journal of the Ceramic Society of Japan 122 [4] 271-275 2014 Paper

Tough and dense boron carbide obtained by high-pressure (300 MPa) and low-temperature (1600°C) spark plasma sintering

Petre BADICA,[*,,***] Salvatore GRASSO,[****] Hanna BORODIANSKA,[*,**] Sky Shumao XIE,[**] Peifeng LI,[**] Peter TATARKO,[****] Mike J. REECE,[****] Yoshio SAKKA[*] and Oleg VASYLKIV[*,**,†]**

[*]National Institute for Materials Science, 1–2–1 Sengen, Tsukuba, Ibaraki 305–0047, Japan
[**]Nanyang Technological University, 50 Nanyang Avenue, 639798 Singapore, Singapore
[***]National Institute of Materials Physics, Atomistilor 105bis, Magurele, 077125, Romania
[****]School of Engineering & Materials Science and Nanoforce Technology Ltd., Queen Mary University of London, Mile End Road, London E1 4NS, UK

Dense boron carbide (above 95%) was achieved through high pressure (300 MPa) and low temperature (1600°C) Spark Plasma Sintering (SPS). This approach resulted in improvement of fracture toughness and of dynamic toughness when compared to corresponding toughness values of the sample sintered by conventional SPS (2100°C, 50 MPa). Dynamic toughness was extracted from Split Hopkinson Pressure Bar measurements. Results are understood based on microstructure and on very different behaviour of the samples in respect to residual B_2O_3 and carbon available in the raw B_4C powder.

Key-words : Boron carbide, High pressure Spark plasma sintering, Dynamic toughness

[Received November 29, 2013; Accepted February 1, 2014]

1. Introduction

Boron carbide hardness at room temperature of 30–60 GPa is considered inferior only to diamond and cubic-BN. Boron carbide is less expensive and easier to prepare. Boron carbide is a strategic material with applications under extreme conditions such as nuclear, protection and space industries. It is also used for cutting and abrasive tools, ceramic bearings, production of refractories, and others. Boron carbide is studied as a candidate for high temperature energy conversion showing thermoelectric properties.[1)] As a semiconductor or metallic compound (depending on its stoichiometry), boron carbide is also of interest for electronics [2–4 and therein refs.].

Excellent properties of boron carbide are the consequence of its strong covalent bonding. Covalent nature is also the reason for the difficult-to-consolidate behaviour of boron carbide. This makes challenging conventional sintering (under normal pressure). A temperature of 1800°C was indicated in ref. 5) to be the temperature where densification starts. Usually, practical sintering temperatures are above 2250°C. Sintering aids can improve densification and some additions can also significantly lower sintering temperature.[3)] However, a large amount of additions also decreases the mechanical properties. Other solutions are the use of pressure-assisted sintering techniques. Popular is hot pressing. Applied pressures are in the range of 20–100 MPa. By this technique applied on powders considered to be pure boron carbide, high relative densities above 95% are attained. But, processing temperature is still high exceeding 2150°C.[6)] Almost fully dense boron carbide samples are achieved by hot isostatic pressing. Pressures (~300 MPa) are higher than for hot pressing, and sintering temperatures are similar (~2150°C).[3)] More recently, spark plasma sintering (SPS) has been demonstrated as an effective technique to achieve high density boron carbide materials. High density boron carbide was obtained by SPS under relatively low pressures of 35[7)] or 120 MPa[8)] at temperatures of 2050–2100 and 1800°C, respectively. Remarkably is that not only lower temperatures were used, but also SPS dwell times (5–10 min) were shorter when compared to other sintering methods.

SPS is a powerful alternative for production of top quality boron carbide samples. However, our comparative analysis is made for samples of very different sizes and shapes. More important is that each work uses boron carbide powders from different suppliers and these powders show very different particle features (size, size distribution, morphology, others) as well as chemical and phase compositions. It is well known that the ratio between boron and carbon of the boron carbide phase can vary within a large range.[2)–4)] In addition, raw powders always contain a relatively high amount of free carbon and that boron carbide particles are usually covered by a layer of a boron oxide phase.[2)–4)] Free B[9)] and C[10)] in the B_4C powders were reported to have a favourable contribution to sintering and nearly fully dense samples were obtained, while boron oxides B_2O_3, B_2O_2 and BO are often mentioned to evaporate[11)] and to hinder sintering.

To have a better understanding of SPS potential for consolidation of boron carbide we used one commercial powder for all experiments. We employed typical SPS conditions such as a high temperature (2100°C) in the lower limit of the values applied in hot or hot isostatic pressing and a moderate pressure (50 MPa) to obtain a dense reference sample. We explore and show that SPS at temperatures as low as 1600°C and at high pressure (300 MPa) is resulting in production of dense samples and toughness of such samples under static and dynamic loads exceed those of the reference sample. Processing and microstructural details leading to these results are discussed.

† Corresponding author: O. Vasylkiv; E-mail: oleg.vasylkiv@nims.go.jp, ovasylkiv@ntu.edu.sg

DOI http://dx.doi.org/10.2109/jcersj2.122.271

Table 1. Samples, SPS regime (maximum temperature/dwell time/maximum pressure), relative density, Vickers hardness, fracture toughness K_{1c}, dynamic SHPB toughness S, SHPB maximum stress σ_{max}, and maximum SHPB strain ε_{max}

Sample	SPS regime	Relative Density (%)	HV (GPa)	K_{1c} (MPa.m$^{1/2}$)	S (MJ/m^2)	σ_{max} (MPa)	ε_{max}
A	1600°C/20 min/300 MPa	95.6	27.6 ± 1.8	6.6 ± 0.7	19.3	1420	0.0171
B	2100°C/10 min/50 MPa	97.8	35.3 ± 2.6	3.8 ± 0.4	5.1	486	0.0146

2. Experimental details

Raw material was commercial B_4C (HD 20, H. C. Starck) with specific surface area of 22–27 m^2/g. According to the manufacturer the N, O, Si impurities were 0.7, 2.6 and 0.15 wt %, respectively.

The powder was sintered using an SPS furnace (FCT HP D 20) under initial vacuum of ~8 Pa. To achieve high pressures during SPS, a device capable of applying a maximum pressure of 500 MPa on a sample of 10 mm in diameter and 7 mm thickness was designed and executed. The device is composed of an outer and an inner graphite die, and the powder is pressed between two SiC punches. Details on the high pressure set up can be found in refs. 12,13. In a typical sintering experiment, 1 g of B_4C powder was poured into the die. The temperature was accurately controlled using a side pyrometer focused on the outer surface of the inner die (i.e., 1 cm far from the sample). Heating and cooling rates during SPS were 50°C/min. Samples and SPS regimes are presented in **Table 1** (see also *section 3 Results and Discussion*).

The density of the samples was determined by Archimede's method and theoretical density of B_4C was taken 2.52 g/cm^3.

X-ray diffraction (XRD) was measured using a Bruker AXS D8 Advance (Germany) diffractomer ($Cu_{K\alpha}$ radiation).

The microstructure was observed by scanning electron microscopy FE-SEM (Jeol JSM-6300).

Vickers indentations were performed for 1 Kg load (Future-Tech FM-300e, Japan) and results were averaged for at least 10 measurements. Static indentation fracture toughness was calculated according to ref. 14: $K_{1c} = 9.052 \times 10^{-}3(HV)^{3/5}Y^{2/5}dl^{-1/2}$, where HV is Vickers hardness, Y is Young's modulus, d is the average diagonal line length of the indentation print, and l is the average length of the cracks.

Uniaxial dynamic compression tests at high strain rates of 1000 s^{-1} were conducted using a Split-Hopkinson Pressure Bar (SHPB) system available at NTU, Singapore. The apparatus consists of 20 mm diameter YAG300 maraging steel striker (length 400 mm), incident and transmitted (both 1200 mm long) bars. The incident and transmitted bars were instrumented with TML strain gauges (Tokyo Sokki Kenkyujo Co. Ltd., Japan, gauge factor of 2.11). Signals from strain gauges were used to calculate the stress and strain history based on the one-dimensional elastic bar wave theory for a pulse propagating in an uniform bar (SHPB theory) as described in ref. 15. Hardened high strength steel plates with impedance matching that of the bars were sandwiched between the bars and specimens to avoid the indentation of the bars.[16] The time duration of the test was of the order of 15–20 μs. SHPB dynamic toughness was determined as the area under the stress–strain curves (see section 3.*Results and Discussion*). Together with SEM, optical microscopy (Leica Stereo Microscope MZ6, Germany) was employed to visualize comminuted samples after SHPB test.

3. Results and discussion

The morphology of the starting powder is shown in **Fig. 1**. Particle size is widely distributed between 0.1 and 1 μm. The master size analysis revealed that 10% of the particles were smaller than 0.3 μm, 50% were smaller than 0.6 μm and 90% were smaller than 1.5 μm. The average particle size is ~0.8 μm. More important is that according to XRD [**Fig. 2**(a)] raw powder is not pure B_4C and impurities of graphite and boron oxide (B_2O_3) are present.

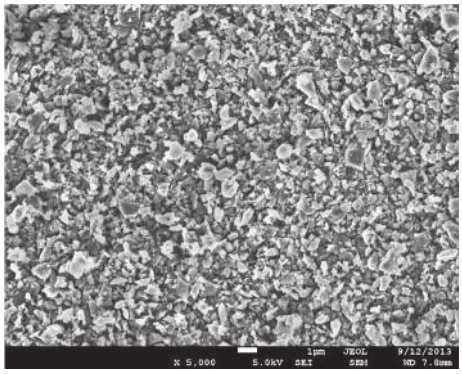

Fig. 1. SEM image of the B_4C raw powder.

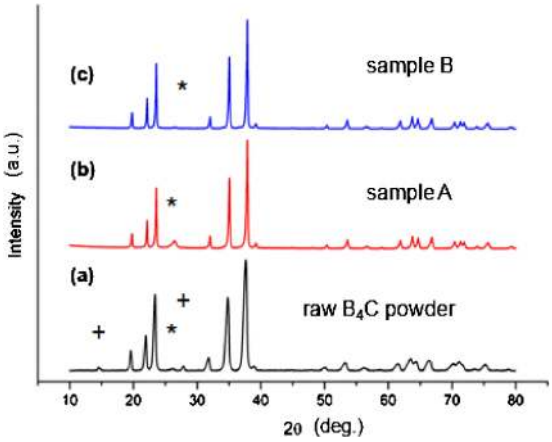

Fig. 2. XRD patterns taken on: (a)-raw powder, (b)-sample A SPSed at 1600°C/300 MPa and (c)-sample B SPSed at 2100°C/50 MPa (see Table 1). Lines marked with (*) are ascribed to graphite (ICDD 75-2078) and with (+) to B_2O_3 (ICDD 13-0570). All the other lines are ascribed to B_4C (ICDD 37-0798).

Figure 3(a) shows the relative punch displacement of the samples during SPS. Punch displacement is proportional with shrinkage of the sample during SPS. In the case of sample A sintered under high pressure (300 MPa), the pressure was linearly increased up to 1200°C and was maintained constant above this temperature. For sample B, SPSed at a low pressure (50 MPa), the maximum pressure was applied at 2100°C and until this temperature pressure was constant at 16 MPa.

It is worth noting that SPS conditions and curves of relative displacement vs. temperature are very different, but both

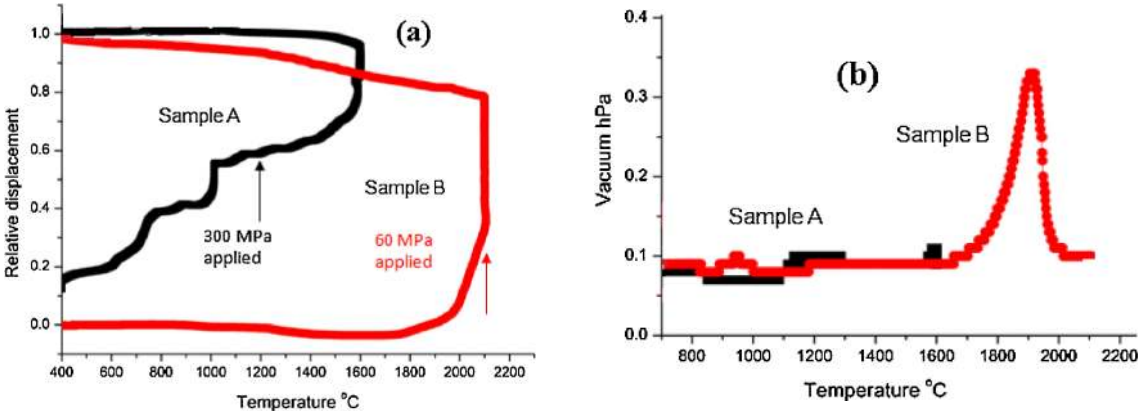

Fig. 3. SPS processing: (a)-relative displacement of the punch vs. temperature and (b)-vacuum pressure in the SPS chamber during heating vs. temperature.

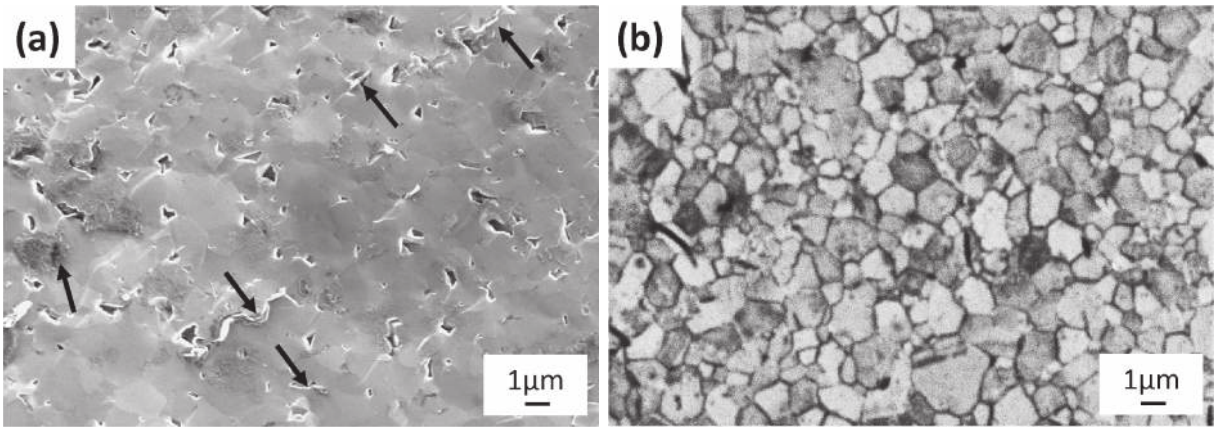

Fig. 4. SEM images of: (a)-sample A and (b)-sample B. Arrows indicate free carbon at the grain boundaries of B_4C. Image on sample B is taken after polishing and chemical etching.

samples A and B show a high relative densification stage. This was attributed to the presence of liquid B_2O_3 which promotes precipitation of B_4C or it is due to the evaporation and condensation of oxide gases such as B_2O_2, BO and CO [3 and therein refs].

Lee and Speyer[17),18)] also observed a slowdown in consolidation rate between 2010 and 2140°C explained by evaporation and condensation of B_4C. The stage of slowdown in densification is not observed in our case although sample B was processed by SPS at similar high temperatures. However, evolution of the vacuum pressure in the SPS furnace during heating [Fig. 3(b)] suggests significant evaporation above 1650°C for sample B and up to about 1900°C.

The temperature of the evaporation end (1900°C) is slightly below 1980°C that is the start temperature of the already mentioned rapid densification for the reference sample B.

This sample shows also weak evaporation at lower temperature of about 950°C. Low temperature evaporation, but shifted to slightly higher temperatures of about 1200–1300°C is observed also for sample A, but the high temperature evaporation stage is likely not reached. XRD from Figs. 2(b), 2(c) shows that the main residual phase in sample A SPSed at low temperature (1600°C) is graphite, while in sample B SPSed at high temperature (2100°C) the amount of impurity phases is low, at traces level. Dacic et al.[11)] for carbothermal reaction of B_2O_3 in the air and under normal conditions found that up to about 1600°C B_2O_3 is in the liquid state and above this temperature decomposes and evaporates into suboxide gas phases. Dacic et al.[11)] also underlined that under vacuum the equilibrium shifts towards formation of the suboxide gas phases. As for carbon, above 1600°C, CO may form and evaporate. We shall remind that we applied vacuum (initial pressure was ~8 Pa) during SPS processing influencing reactions, stability domains and evaporation. These complex processes are also influenced by application of the SPS pressure producing at least a different sintering versus gas squeezing behaviour. Other details that may also contribute are the SPS activation electric field assisted specific features[19)–24)] such as formation of hot spots and occurrence of electro diffusion, generation of sparks and of debatable plasma states leading to grain boundary cleaning, and heating from inside to outside as for microwave sintering. In summary, presented analysis of literature data and of our results suggest that low temperature evaporation can be ascribed mainly to B_2O_3 evaporation, while the one at higher temperature is mainly due to carbon evaporation. This result is supported by EDS measurements performed on the area of the sample's surface visualized at magnifications of 500 or 1000 times. Average B/C ratio was calculated for about 8–12 measurements for each sample. There is indeed a relative and apparent enrichment with carbon in sample A comparative to raw powder so that the B/C ratio decreases from 3.7–3.9 in the raw powder to 3.2–3.3 in sample A. The ratio B/C in sample B is the highest at 4.1–4.3. It is worth noting that precision of

EDS in concentration determination of light-weight elements is low and our data should be regarded as qualitative. The presence of carbon in sample A can be also observed by SEM in **Fig. 4**(a).

Presented results indicate that sample A can be considered a B_4C–C composite, while sample B is a B_4C almost pure ceramic. This results in the expectations that mechanical properties are different. The presence of carbon in sample A introduces plasticity and the consequences are:

(i) Sample A has a lower *HV*, but still at competitive values (Table 1).

(ii) There is an enhancement of static and dynamic toughness (Table 1, **Fig. 5**) for sample A containing carbon. Enhancement of static indentation toughness, K_{1c}, was found in another hard bulk ceramic Si_3N added with graphene and produced by SPS.[25] For many B_4C-based composites enhancement of static toughness was observed and sometimes this is not accompanied by the decrease of hardness. A recent example is for B_6O–B_4C composites obtained by SPS.[26]

Enhancement of toughness in sample A cannot be solely attributed to the presence of free carbon at grain boundaries. A smaller grain size will provide more grain boundaries that can influence mechanical properties improving toughness. The average grain size is higher for our samples A (1.2 µm) and B (1.7 µm) when compared to raw powder (0.8 µm) [see also Fig. 1 and Fig. 4(b)]. The highest average grain size was found for sample B produced at high temperature (2100°C). Nevertheless the differences in the average grain size are not very high and grain size uniformity is good for both samples A and B. This provides the argument to assume that the main contribution to toughness enhancement in sample A is mainly due to the presence of free carbon.

Samples after SHPB test were observed by optical microscopy and SEM. Large pieces were found after SHPB test for both samples. Our experience on B_4C-based ceramic produced by reactive SPS under N_2 atmosphere[27] showed that enhancement of *S* owing mainly to the increase in σ_{max} as for the samples from this work is accompanied by fracturing into large pieces. A relatively large fraction of small particles was found when *S* enhancement is accompanied also by a significant enhancement of ε_{max}. Indeed, for the samples from A and B the fine particles fraction was small, as expected for a small increase of ε_{max} (Table 1), but sample A shows some tendency in this respect. In **Fig. 6** curved or round shape surfaces can be observed for sample A. For sample B straight fracture lines and sharp edges form.

Our attempts to observe SHPB fracture edges, lines and surfaces versus EDS compositional maps or macro defects such as pores have indicated that there is no direct obvious correlation between the dynamic response of the samples and morphology details of the comminuted samples. A similar result was found for the samples of B_4C obtained by reactive SPS in N_2 atmosphere and all discussions and results from our article[27] are supported by the data from this work. The only difference is that in this work *HV* is somehow smaller for a higher σ_{max} and *S* (Table 1). Further systematic and detailed investigation of the complex relationships between processing, microstructure, static, and dynamic mechanical properties is necessary.

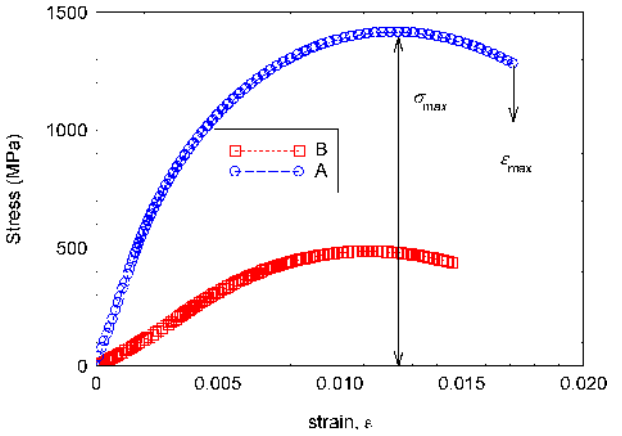

Fig. 5. SHPB stress–strain curves for SPSed samples A and B (notation from Table 1). Arrows indicate how the values of σ_{max} and ε_{max} (see Table 1) were estimated.

4. Conclusion

It is shown that high pressure (300 MPa) and low temperature (1600°C) SPS can produce samples with improved static and dynamic toughness, while Vickers hardness and bulk density are quite high. These samples have a lower grain size and a certain relatively high amount of free carbon when compared to reference sample produced by SPS under usual conditions (50 MPa and at 2100°C).

Results suggest the possibility of toughness control of B_4C-based ceramic through the proposed SPS new approach, but it also emphasizes the importance of the raw powder quality. Impurity phases and interfaces (free C and B_2O_3) on the surface of B_4C particles and their evolution during SPS deserve further attention towards ceramic optimization and improvement.

Acknowledgement S.G. and M.J.R. acknowledge EP/K008749/1, UK, and PB acknowledges PCCE 3/2012, Romania.

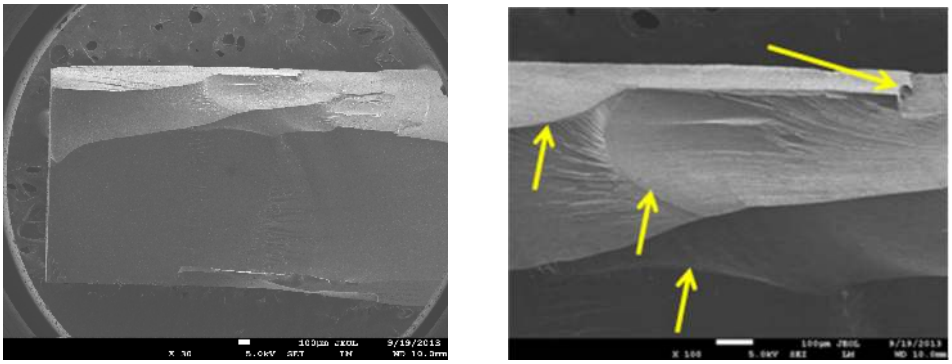

Fig. 6. Sample A after SHPB test: SEM general image (left) and detail (right). Arrows indicate curved fracture lines and surfaces.

References

1) M. Bouchacourt and F. Thevenot, *J. Mater. Sci.*, 20, 1237–1247 (1985).
2) F. Thevenot, *J. Eur. Ceram. Soc.*, 6, 205–225 (1990).
3) A. K. Suri, C. Subramanian, J. K. Sonber and T. S. R. Ch. Murthy, *Int. Mater. Rev.*, 55, 4–40 (2010).
4) V. Domnich, S. Reynaud, R. A. Haber and M. Chhowalla, *J. Am. Ceram. Soc.*, 94, 3605–3628 (2011).
5) H. Lee and R. F. Speyer, *J. Am. Ceram. Soc.*, 86, 1468–1473 (2003).
6) D. Jianxin and S. Junlong, *Ceram. Int.*, 35, 771–778 (2009).
7) S. Grasso, C. Hu, O. Vasylkiv, T. S. Suzuki, S. Guo, T. Nishimura and Y. Sakka, *Scr. Mater.*, 64, 256–259 (2011).
8) O. Vasylkiv, H. Borodianska, P. Badica, S. Grasso, Y. Sakka, A. Tok, L. T. Su, M. Bosman and J. Ma, *J. Nanosci. Nanotechnol.*, 12, 959–965 (2012).
9) J. E. Zorzi, C. A. Perottoni and J. A. H. da Jornada, *Mater. Lett.*, 59, 2932–2935 (2005).
10) B. Y. Yin and L. S. Wang, *J. Inorg. Mat.*, 18, 633–637 (2003).
11) B. Z. Dacic, V. Jokanovic, B. Jokanovic and M. D. Dramicanin, *J. Alloys Compd.*, 413, 198–205 (2006).
12) S. Grasso, B. N. Kim, C. Hu, G. Maizza and Y. Sakka, *J. Am. Ceram. Soc.*, 93, 2460–2462 (2010).
13) S. Grasso, J. Poetschke, V. Richter, G. Maizza, Y. Sakka and M. J. Reece, *J. Am. Ceram. Soc.*, 96, 1702–1705 (2013).
14) K. Niihara, R. Morena and D. P. H. Hasselman, *J. Mater. Sci. Lett.*, 1, 13–16 (1982).
15) U. S. Lindholm, *J. Mech. Phys. Solids*, 12, 317–335 (1964).
16) S. Sarva and S. Nemat-Nasser, *Mater. Sci. Eng., A*, 317, 140–144 (2001).
17) H. Lee and R. F. Speyer, *J. Am. Ceram. Soc.*, 86, 1468–1473 (2003).
18) R. F. Speyer and J. Lee, *J. Mater. Sci.*, 39, 6017–6021 (2004).
19) Z. A. Munir, U. Anselmi-Tamburini and M. Ohyanagi, *J. Mater. Sci.*, 41, 763–777 (2006).
20) S. H. Risbud, J. R. Groza and M. J. Kim, *Philos. Mag. B*, 69, 525–533 (1994).
21) J. R. Groza and A. Zavaliangos, *Mater. Sci. Eng., A*, 287, 171–177 (2000).
22) R. Chaim, M. Levin, A. Slayer and C. Estournes, *Adv. Appl. Ceramics*, 107, 159–170 (2008).
23) P. Badica, A. Crisan, G. Aldica, K. Endo, H. Borodianska, K. Togano, S. Awaji, K. Watanabe, Y. Sakka and O. Vasylkiv, *Sci. Technol. Adv. Mater.*, 12, 013001 (2011).
24) D. Demirskyi, H. Borodianska, D. Agrawal, A. Ragulya, Y. Sakka and O. Vasylkiv, *J. Alloys Compd.*, 523, 1–10 (2012).
25) L. S. Walker, V. R. Marotto, M. A. Rafiee, N. Koratkar and E. Corral, *ACS Nano*, 5, 3182–3190 (2011).
26) I. Solodkyi, S. S. Xie, T. Zhao, H. Borodianska, Y. Sakka and O. Vasylkiv, *J. Ceram. Soc. Japan*, 121, 950–955 (2013).
27) P. Badica, H. Borodianska, S. Xie, T. Zhao, D. Demirskyi, P. Li, A. I. Y. Tok, Y. Sakka and O. Vasylkiv, *Ceram. Int.*, 40, 3053–3061 (2014).